Journal of Metals, Materials and Minerals, 34(2), 1825, 2024

The mechanochemistry of lanthanum dihydride (LaH_2) with hydrogen (H_2) using the ball-mill process and the effect of oxidation on the resulting products

Andika Widya PRAMONO[1,*], Satrio HERBIROWO[1], Agung IMADUDDIN[1], Iwan Dwi ANTORO[1], Heri NUGRAHA[2], Hendrik[3], Anung SYAMPURWADI[1], Ines Hayatun NUFUS[4], Nihayatul UMNA[4], Silvia Farah DIBA[4], and Fina Fitratun AMALIYAH[4]

[1] *Research Center for Advanced Materials – National Research and Innovation Agency (BRIN), Kawasan Puspiptek, Tangerang Selatan 15314, Banten, Indonesia*

[2] *Research Center for Energy Conversion and Conservation - National Research and Innovation Agency (BRIN), Kawasan Puspiptek, Tangerang Selatan 15314, Banten, Indonesia*

[3] *Research Center for Metallurgy - National Research and Innovation Agency (BRIN), Kawasan Puspiptek, Tangerang Selatan 15314, Banten, Indonesia*

[4] *Physics Study Program, Universitas Islam Negeri Sultan Maulana Hasanuddin, Gedung Dekanat Fakultas Sains, Kampus 2, Jalan Syekh Moh. Nawawi Albantani, Kemanisan, Kec. Curug, Kota Serang 42171, Banten, Indonesia*

***Corresponding author e-mail**: andi010@brin.go.id

Received date:
29 August 2023
Revised date
12 March 2024
Accepted date:
26 March 2024

Keywords:
Ball-mill process;
Hydrogen storage;
Lanthanum hydride;
Mechanochemistry;
Oxidation

Abstract

The complex behavior of LaH_2 during ball milling was investigated in this study, with its mechanical, chemical, and morphological changes explored. The relationship between milling time and hydrogen pressure reduction was uncovered through detailed experiments, reflecting the dynamic nature of the process. A transient yet significant event was observed upon unsealing the milling jar post-milling: the emergence of a minor fire ember, indicative of the interplay between mechanical forces and chemical reactivity within the LaH_2 powder. Profound changes in the structure, composition, and shape were unraveled using advanced techniques such as X-ray diffraction (XRD), scanning electron microscopy coupled with energy-dispersive X-ray spectroscopy (SEM/EDX), and particle size distribution analysis. The resulting powder exhibited a dual-phase composition of lanthanum dihydride (LaH_2, 68.1% to 71.5%) and lanthanum oxide (La_2O_3, 28.5% to 31.9%), reflecting a dynamic chemical equilibrium during milling. Particle size distribution analysis revealed a notable increase in average diameter to 6420 nm, accompanied by a polydispersity index (PDI) of 0.831, signifying a broadening compared to the initial LaH_2 powder. The morphological evolution of the powder was elucidated through SEM imaging, showing predominantly spherical and rounded forms, indicating extensive particle agglomeration and plastic deformation during milling. Additionally, the formation of oxide layers on the powder surface, intertwined with pronounced particle agglomeration, was highlighted through EDX mapping, shedding light on the mechanical aspects of morphological evolution during milling. These findings contribute to our understanding of LaH_2 behavior under extreme mechanical and chemical conditions and have implications for materials processing, hydrogen storage technologies, and broader applications in materials science and engineering.

1. Introduction

In recent decades, mechanochemistry has emerged as a versatile and innovative approach in materials science and solid-state chemistry [1-3]. This technique utilizes mechanical forces, like milling or grinding, to initiate chemical reactions in solid-state systems [4,5] operating under ambient conditions and offering numerous advantages over traditional synthetic methods. Mechanochemistry efficiently promotes chemical transformations by imparting kinetic energy to reactant particles, facilitating bond-breaking and atomic rearrangement [6-10]. This accelerated kinetics allows for the rapid synthesis of complex materials, making mechanochemistry attractive for on-demand production [7,11]. Moreover, mechanochemistry reduces energy consumption and carbon footprint by eliminating the need for high-temperature furnaces or pressure vessels [12,13]. Unlike solvent-based reactions, it generates minimal waste and avoids environmental contamination, promoting a cleaner approach to materials synthesis [14-16]. Mechanochemistry induces unique structural modifications, forming metastable phases and nanostructures inaccessible through conventional methods [6,17]. These structures often exhibit enhanced

properties suitable for various applications, including catalysis, electronics, and energy storage [9,18,19]. Solvent-free reactions in mechanochemistry preserve sample integrity, eliminating solvent-induced side reactions and ensuring product purity and reliability [20-25]. Consequently, materials synthesized via mechanochemistry demonstrate superior performance and stability, making them desirable for industrial and technological applications [26-28].

Mechanochemistry has evolved as a pioneering technique in materials science and solid-state chemistry, enabling advanced materials' efficient and eco-friendly synthesis [29-31]. The unique combination of accelerated reaction kinetics, reduced energy consumption, and the absence of volatile solvents makes mechanochemistry an attractive and sustainable alternative to conventional synthetic methods [32-34]. As we delve deeper into the potential applications of mechanochemistry, this paper focuses on investigating the mechanochemical behavior of lanthanum dihydride (LaH_2) with hydrogen (H_2) using the ball-mill process, contributing to the growing body of knowledge in the field of sustainable and green energy storage materials.

LaH_2 stands out as a material of considerable significance within the realm of mechanochemistry. Its potential as a hydrogen storage material has attracted widespread attention owing to its high hydrogen content, making it a promising candidate for addressing the challenges of hydrogen storage and utilization in clean energy applications [35-37].

Hydrogen, with its exceptional energy density and potential as a clean fuel, has been recognized as a crucial element in the transition toward a sustainable energy landscape. Hydrogen fuel cells and energy storage systems have emerged as key technologies in pursuing a carbon-neutral society [38-40]. However, the efficient storage and release of hydrogen represent formidable hurdles in realizing the full potential of hydrogen-based energy solutions [41-43].

The thermodynamics of the hydrogen desorption and absorption reactions in LaH_2 pose considerable hurdles, rendering its handling and manipulation with conventional methods challenging [44,45]. The high energy barrier associated with the hydrogen desorption process necessitates elevated temperatures to drive the reaction [45-47], making it energy-intensive and impractical for real-world applications. Furthermore, the slow hydrogen release and absorption kinetics in LaH_2 significantly restrict the material's overall efficiency and responsiveness as a hydrogen storage medium [48,49].

In this context, the application of mechanochemistry represents a promising solution to overcome the inherent limitations of LaH_2. The ball-mill process, a well-established mechanochemical technique, can provide the necessary mechanical energy to activate and accelerate the hydrogen desorption and absorption reactions in LaH_2. By employing mechanical forces to drive these reactions, the need for high temperatures can be circumvented, allowing for the manipulation of LaH_2 under milder conditions, thereby improving its practicality as a hydrogen storage material.

By delving into the mechanochemical behavior of LaH_2 with H_2, this research aims to uncover the fundamental mechanisms that govern the hydrogen desorption and absorption kinetics in LaH_2. This investigation is vital to understand the intricate factors influencing the hydrogen storage properties and to identify the potential challenges associated with the mechanochemical synthesis of LaH_2-based hydrogen storage materials.

The interest in LaH_2 within the domain of mechanochemistry is fueled by its remarkable hydrogen storage capacity and its potential applications in hydrogen fuel cells and energy storage systems. However, the thermodynamic challenges of hydrogen desorption and absorption limit its handling with conventional methods. This research seeks to leverage mechanochemistry to gain insight into the hydrogen storage behavior of LaH_2, paving the way for the development of more efficient and practical hydrogen storage materials for sustainable energy applications.

In the quest to overcome the challenges associated with LaH_2 as a hydrogen storage material, the ball-mill process emerges as a highly promising and well-established mechanochemical technique. The ball-mill process harnesses the power of high-energy collisions between milling balls and the reactant powder, initiating mechanical activations that enhance chemical reactivity and reaction efficiency [50-52].

The ball-mill process is conducted within a sealed container, ensuring a controlled and inert environment. This setup prevents the loss of reactants and the introduction of impurities, guaranteeing the purity and reliability of the reaction products. Milling balls are set into rapid motion inside the ball mill, creating high-impact collisions with the LaH_2 powder. These high-energy collisions impart mechanical energy to the reactant particles, breaking chemical bonds and promoting atomic rearrangements in the material [53-55].

The key advantage of the ball-mill process lies in its ability to enable chemical reactions to occur under milder conditions than conventional thermal methods. Unlike the traditional high-temperature treatments required for hydrogen desorption and absorption, the ball-mill process achieves mechanical activation, circumventing the need for elevated temperatures. As a result, this technique offers the potential for more energy-efficient and practical hydrogen storage solutions [56,57].

Furthermore, the ball-mill process promotes the formation of nanocrystalline structures and metastable phases, which may not be readily accessible through conventional methods [58-60]. These unique structures offer improved hydrogen storage properties and can significantly enhance the overall performance of a hydrogen storage material.

The ball-mill process offers a versatile solution for LaH_2 hydrogen storage challenges. It enhances reactions, aiding efficient storage material development. Exploring LaH_2-H_2 mechanochemistry via ball-milling deepens kinetic understanding, aiding clean energy tech design.

While several studies have explored the mechanochemical behavior of various materials, there is a dearth of comprehensive investigations on the mechanochemistry of LaH_2 with H_2 using the ball-mill process. The novelty of this research lies in its focused examination of the mechanochemical reactions in LaH_2-H_2 systems. The primary objective of this scientific paper manuscript is to explore the mechanochemistry of LaH_2 with H_2 using the ball-mill process. The specific aims include:

- Characterizing some initial LaH_2 powder properties, such as crystal structure, particle morphology, and particle size.
- Investigating and analyzing the rate of hydrogen pressure depletion during the ball-mill process.
- Characterizing and analyzing the resultant ball-milled powder material properties after the ball-mill process, such as crystal structure, particle morphology, and particle size.

2. Experimental

2.1 Initial LaH_2 powder and H_2 gas

This study used LaH_2 powder with the brand EASCHEM, i.e., Changsha Easchem Co. Ltd China, with a purity of 99.95% or 3 N and CAS No. 13864-01-2. The average particle size and distribution of this LaH_2 powder were analyzed using the *Nanoplus Particulate System*. The composition and crystal structure of LaH_2 powder were investigated using X-ray diffraction (XRD) analysis with XRD PANalytical Empyrean. The XRD PANalytical Empyrean measurement used Cu anode with $K_{\alpha1}$ = 1.541 Å, $K_{\alpha2}$ = 1.544 Å, K_{β} = 1.392 Å. The scan was conducted within the range of $5.012° \leq 2\theta \leq 84.982°$ and the 2θ-step size of 0.022° for 23.97 s at 25°C. The morphology of LaH_2 powder was observed using a scanning electron microscope (SEM) and energy dispersive X-ray spectrometer (EDX) of Hitachi SU3500. The H_2 gas used had a purity of 99.999%.

2.2 Ball-mill

The ball mill was conducted in a stainless steel jar equipped with a manometer and gas inlet-outlet on the lid. The jar's inner volume was measured to be 581.9 cm^3, while the total volume of the small stainless steel milling balls was 21.0 cm^3 weighing 155.747 g. The milling balls were chosen for their tiny size, providing a large total surface area. The m_{ball}/m_{LaH2} ratio was determined to be 19.818 using 155.747 g of milling balls and 7.859 g of LaH_2.

Before milling, the stainless steel jar and balls were cleaned with ethanol and air-dried. Then, 7.859 g of LaH_2 powder and milling balls were added to the jar. An air compressor created a vacuum, ensuring no air pressure in the sealed jar. After introducing 9.65 bar of H_2 gas, the jar was placed in the FILA ball-mill device (Figure 1). Operating at 130 rpm, the machine dry-milled continuously.

Throughout the milling process, the change in H_2 pressure inside the jar was monitored using the digital manometer (Figure 2) and recorded when the milling machine was paused. On average, monitoring the change in H_2 pressure was conducted twice a day, i.e., in the morning and the afternoon. The milling was finally stopped once the pressure inside the jar became 0 bar, indicated by the digital manometer.

After the milling process, the resultant ball-milled powder was emptied from the jar. The CILAS 1190 was employed to assess the average particle size and distribution of the produced ball-milled powder. Two rounds of X-ray diffraction (XRD) analysis were conducted on the resulting powder using the XRD PANalytical Empyrean instrument. In the first measurement, a Cu anode with specific wavelengths ($K_{\alpha1}$ = 1.541 Å, $K_{\alpha2}$ = 1.544 Å, and K_{β} = 1.392 Å) was utilized. The XRD scan encompassed the range of $5.012° \leq 2\theta \leq 84.982°$, employing a step size of 0.022°, and the scanning step was sustained for 23.97 s at a temperature of 25°C. Similarly, for the second measurement, a Cu anode with specific wavelengths was utilized. The second XRD scan covered the range of $10.013° \leq 2\theta \leq 79.979°$, utilizing a step size of 0.026°, and the scanning step lasted for 22.44 s at 25°C. Additionally, scanning electron microscopy (SEM) observation and energy-dispersive X-ray (EDX) analysis were conducted using the JEOL JSM-IT200. Table 1 summarizes the important parameters of the conducted experiment of ball-mill LaH_2 powder with H_2 gas.

Figure 1. FILA ball-mill machine.

Figure 2. Digital manometer on the lid of the milling jar.

Table 1. The parameters of the ball-mill experiment of LaH2 plus H2.

No.	Item	Amount	Test
1	Mass of LaH_2 powder	7.859 g	PSA (particle size analysis), XRD analysis, and SEM/EDX analysis
2	The pressure of H_2 gas	9.65 bar	
3	Ratio of m_{ball}/m_{LaH2}	19.818	
4	Average ball-mill rotation	130 rpm	
5	The volume of the milling jar	581.9 cm^3	
6	Mass of milling balls	155.747 g	
7	The volume of milling balls	21.0 cm^3	
8	Resultant ball-milled powder		PSA (particle size analysis), XRD analysis, and SEM/EDX analysis

3. Results and discussion

3.1 Initial LaH_2 powder

3.1.1 Particle size distribution

Figure 3 and Table 2 display the results of the particle size analysis conducted on the initial LaH_2 powder. The polydispersity index (PDI) presented in Table 2 is a dimensionless parameter used to assess the width of the particle size distribution. A lower PDI value indicates a more uniform and narrower distribution, while a higher PDI value suggests a broader range of particle sizes [61-63]. The percentile values (D(10%), D(50%), and D(90%)) in Table 2 represent specific points in the particle size distribution [64-66]. For example, D(10%) corresponds to the diameter below which 10% of the particles in the sample, by volume or number, are present. D(50%), also known as the median diameter, signifies the diameter below which 50% of the particles lie, effectively dividing the distribution into two halves. D(90%) indicates the diameter below which 90% of the particles are found.

Normalized intensity distributions of three attempts (Figure 3) showed consistent, narrow, bell-shaped curves for the initial LaH_2 powder. Average particle size from all attempts: 695.6 nm. Calculated PDI: 0.274, indicating moderately narrow size distribution, implying uniformity. Average D(10%), D(50%), D(90%): 500.6 nm, 605.6 nm, 735.5 nm, respectively. This reveals insights on particle size range: 90% below 735.5 nm and 10% below 500.6 nm.

The particle size analysis of the initial LaH_2 powder indicated a relatively narrow size distribution with particles centered around a median diameter of approximately 605.6 nm. Understanding such physical characteristics is crucial for optimizing processes or applications that rely on precise particle size control.

3.1.2 XRD analysis

Figure 4 displays the diffractogram obtained from the initial LaH_2 powder. The most prominent diffraction peak for LaH_2 occurred at $2\theta = 27.5268°$ in the 111-direction. This finding aligns with previous observations reported by Machida *et al*. [67], who mentioned the 111-reflection of LaH and $LaH_{2+\delta}$ phases, and Boroch *et al*. [68], who reported on LaH_2 and LaH_3.

Table 3 provides a detailed account of the XRD results, listing the identified patterns. The Rietveld analysis revealed that the initial powder consisted of 98.0% LaH_2 (identified with compound code 9009020) with a stoichiometry of La_4H_8, and 2.0% pure La metal (identified with compound code 9010986) with a stoichiometry of $La_{2.00}$. The high presence of 98.0% LaH_2 (Figure 4) confirmed that the primary constituent of the sample was lanthanum hydride. The scale factor of 0.054 indicated the adjustment of the intensity of the diffraction peaks for this compound during the analysis to match the reference pattern. The detection of 2.0% pure La metal (Figure 4) suggested the presence of a minor impurity or unreacted lanthanum in the sample. The scale factor of 0.078 indicated that the intensity of the diffraction peaks for this metal was also adjusted to match the reference pattern. This La presence might stem from incomplete chemical reactions during the synthesis or preparation process of the LaH_2 powder.

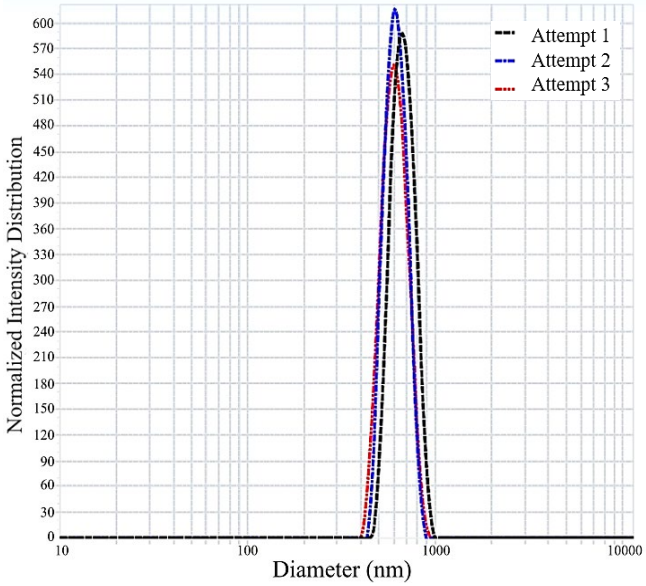

Figure 3. Normalized particle size distribution of the initial LaH_2 powder.

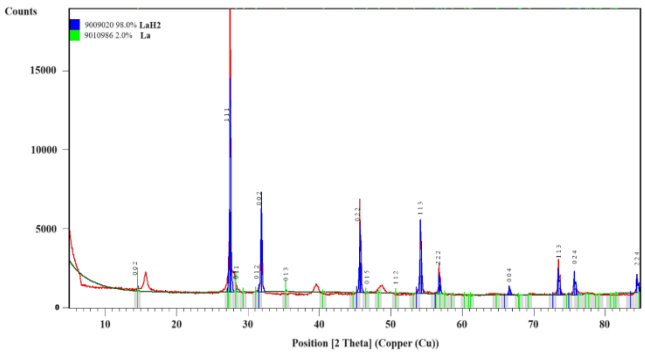

Figure 4. X-ray diffractogram and Rietveld analysis of the initial LaH_2 powder.

Table 2. The statistics of particle size analysis of the initial LaH_2 powder through the *Nanoplus Particulate System*.

Attempt no.	Average diameter (nm)	Polydispersity index (PDI)	Percentile D (10%) (nm)	Percentile D (50%) (nm)	Percentile D (90%) (nm)
1	762.8	0.312	531.8	643.3	780.4
2	671.1	0.286	494.0	590.7	709.4
3	652.8	0.224	476.1	582.9	716.7
Average	695.6	0.274	500.6	605.6	735.5

Table 3. Identified pattern list of the initial LaH_2 powder.

Visible	Ref. node	Score	Compound name	Displacement [°2Th.]	Scale factor
*	96-900-9021	17	9009020	0.000	0.054
*	96-901-0987	5	9010986	0.000	0.078

3.1.3 SEM and EDX analysis

Figure 5 shows the morphology of the initial LaH_2 powder under scanning electron microscopy (SEM) examination. From Figure 5(a) it is obvious that the initial LaH_2 powder consisted primarily of fine particulates, despite the presence of a few large particles. This finding is in line with the results of particle size analysis (PSA), in Figure 3 and Table 2, indicating a relatively narrow size distribution with particles centered around a median diameter of approximately 605.6 nm. Referring to some literature [69-72], this initial LaH_2 powder took primarily the shapes of angular, acicular, and flaky regardless of size (Figure 5(b-d)).

Figure 6 shows the result of the EDX analysis. It was found that there were some layers of oxide on the surface of the initial LaH_2 powder (Figure 6(a)), shown by red areas. In the specific area observed, the amount of oxygen was 15.8 wt% (Figure 6(b)) or 62.1 at% (Figure 6(c)). When metallic powders are exposed to the atmosphere, they come into contact with oxygen molecules present in the air. Metals tend to lose electrons, and oxygen has a high affinity for gaining electrons [73,74]. In the presence of oxygen, the metal atoms in the powder release electrons to the oxygen molecules. This electron transfer leads to the formation of metal cations (positively charged metal ions) and oxygen anions (negatively charged oxygen ions). The metal cations combine with the oxygen anions to form metal oxide compounds. These metal oxide compounds coat the surface of the metal particles and create a layer of oxide. These oxide layers might have a detrimental effect on the resultant ball-milled powder after ball-mill.

3.2 Change in H_2 pressure over milling time

As the H_2 gas reacted with LaH_2 during the ball mill, the number of hydrogen atoms absorbed by LaH_2 was proportional to the decrease of hydrogen pressure inside the milling jar. The behavior of the decrease of H_2 pressure (p) with time (t) followed some polynomial trends, having the coefficient of determination (R^2) very close to or equal to 1. Constrained to the positive x-y axes and with the degree of polynomial $n \geq 3$, there were some possible polynomial equations with R^2 very close to or equal to 1 for this p-t performance as follows:

$$P = -8.10^{-7}t^3 + 0.0005t^2 - 0.1113t + 9.2905; \quad R^2 = 0.9994 \text{ (Figure 7(a))} \tag{1}$$

$$P = 2.10^{-9}t4 - 2.10^{-6}t^3 + 0.00007t^2 - 0.1228t + 9.4481; \quad R^2 = 0.9999 \text{ (Figure 7(b))} \tag{2}$$

$$P = -1.10^{-11}t^5 + 1.10^{-8}t^4 - 4.10^{-6}t^3 + 0.0009t^2 - 0.1295t + 9.4945; \quad R^2 = 1 \text{ (Figure 7(c))} \tag{3}$$

$$P = 1.10^{-14}t^6 - 2.10^{-11}t^5 + 1.10^{-8}t^4 - 4.10^{-6}t^3 + 0.0009t^2 - 0.13t + 9.4961 \quad R^2 = 1 \text{ (Figure 7(d))} \tag{4}$$

Where: p = H_2 pressure (bar) t = milling time (h)

The duration of ball-mill $LaH_2 + H_2$ until the H_2 pressure became zero was 252.765 h or equal to 10 days, 12 h, 45 min, and 55 s. It was considered very long for the ball-mill process conducted at room or ambient temperature. The rate of hydrogen absorption by LaH_2 can be increased at elevated temperatures as in the case of hydrogen absorption by Mg 50 wt% $LaNi_5$ composite after mechanical milling [75], or hydrogen diffusion onto lanthanum hydride thin film coated with palladium (Pd) [76].

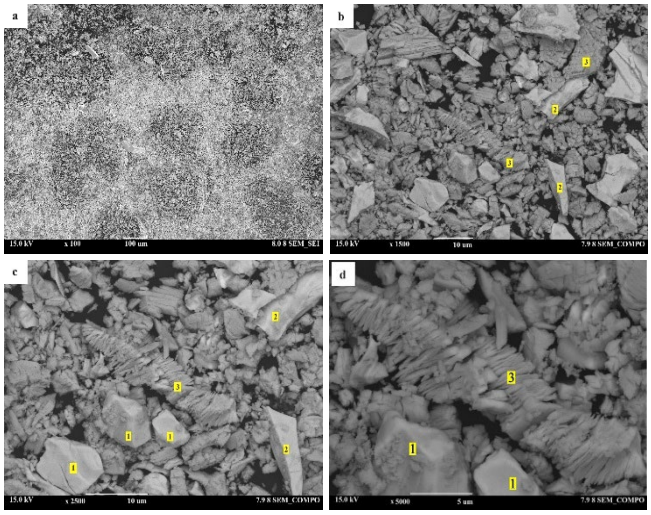

Figure 5. The morphology of the initial LaH_2 powder under SEM observation: (a) 100×, (b) 1500×, (c) 2500×, and (d) 5000×. The shapes of the powder were mainly angular (1), acicular (2), and flaky (3) regardless of size.

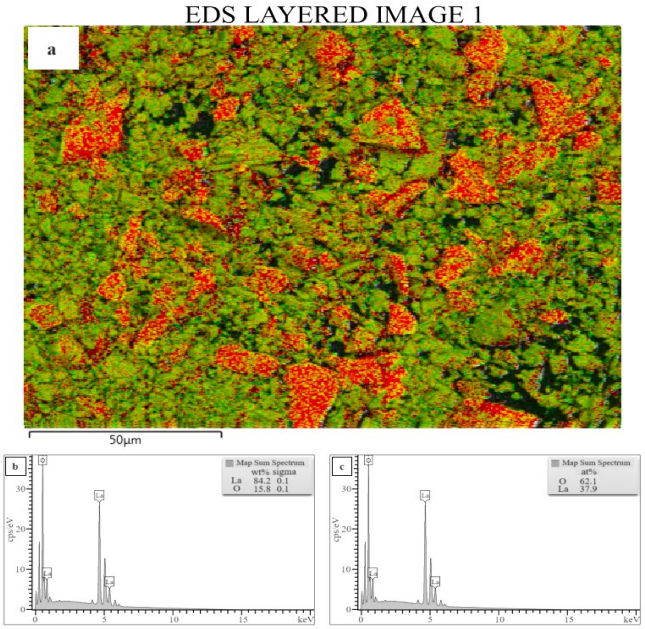

Figure 6. The results of EDX analysis on the initial LaH_2 powder (magnification: 800×): (a) The presence of oxide layers is indicated by red areas, (b) wt% of oxygen, and (c) at% of oxygen.

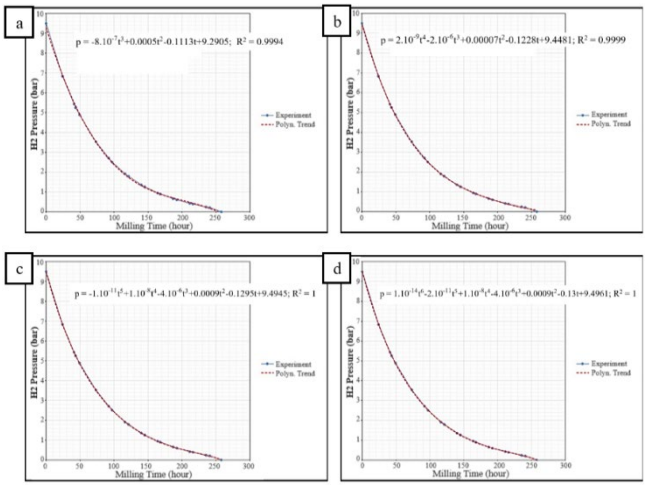

Figure 7. The polynomial fittings for the pressure-temperature (p-t) behavior of ball-mill $LaH_2 + H_2$: (a) n =3, (b) n = 4, (c) n = 5, and (d) n = 6.

Figure 8. A minor fire ember (arrow) in the resultant ball-milled powder.

The absorption rate of hydrogen by lanthanum hydride during ball-mill can vary based on factors such as the milling time, milling speed, and the specific surface area of the materials. In general, a ball-mill increases the surface area of the hydride and enhances the exposure of the material to hydrogen gas, promoting faster hydrogen absorption kinetics. Mechanical forces generated during the ball mill can also induce defects and dislocations in the hydride lattice, which can provide additional pathways for hydrogen diffusion and absorption.

Lanthanum hydride demonstrates non-stoichiometric behavior when exposed to higher temperatures. This non-stoichiometry arises due to the hydrogen's movement away from the octahedral positions within the hydride lattice of the fluorite structure. Importantly, this occurs without the obligatory formation of Schottky defects in the lanthanum lattice of the hydride [77]. The energy for generating a hydrogen vacancy has been quantified through thermal expansion data, revealing a value of 0.10 eV [77]. This case is a measure of the energy barrier for hydrogen diffusion or vacancy formation. This energy barrier determines how fast hydrogen atoms can move within the lattice and how easily vacancies can be formed. Lower energy barriers generally correspond to faster diffusion and absorption kinetics [78,79].

The combination of non-stoichiometry and the energy required for vacancy creation at elevated temperatures can significantly impact the rate of hydrogen absorption by lanthanum hydride. The presence of non-stoichiometry means that there are available sites for hydrogen absorption and movement even without forming defects. The low energy barrier for vacancy creation suggests that hydrogen atoms can move relatively freely within the lattice, leading to faster diffusion and absorption rates. Hydrogen atoms can move in and out of the hydride lattice more easily, facilitating rapid absorption.

The existence of non-stoichiometric phases and the low energy barrier can collectively enhance the overall kinetics of hydrogen absorption. The movement of hydrogen within the lattice without the necessity of forming defects allows for a more rapid exchange of hydrogen atoms between the lattice and the surrounding environment. The non-stoichiometric behavior and energy barriers can also be temperature-dependent. At higher temperatures, thermal energy contributes to overcoming energy barriers, further accelerating hydrogen diffusion and absorption.

3.3 Opening of the milling jar lid

Following the cooling of the milling jar, its lid was taken off within the ambient atmosphere. As the resultant powder was extracted, a minor fire ember emerged within the powder (Figure 8). It is plausible that the heat produced during the milling procedure, in conjunction with variables such as friction or residual heat, prompted a momentary ignition within the powder upon exposure to the air. This occurrence could potentially arise from the existence of combustible particles or materials within the powder.

3.4 Resultant ball-milled powder

3.4.1 Particle size distribution

Three attempts were conducted to examine the particle size along with its distribution for the resultant ball-milled powder using CILAS 1190. Table 4 summarizes the results of the three attempts at particle size analysis.

Table 4. The statistics of particle size analysis of the resultant ball-milled powder through CILAS 1190.

Attempt no.	Average diameter (nm)	Polydispersity index (PDI)	Percentile D (10%) (nm)	Percentile D (50%) (nm)	Percentile D (90%) (nm)
1	6450	0.835	330	3640	16420
2	6400	0.812	290	3590	16330
3	6410	0.847	350	3630	16210
Average	6420	0.831	320	3620	16320

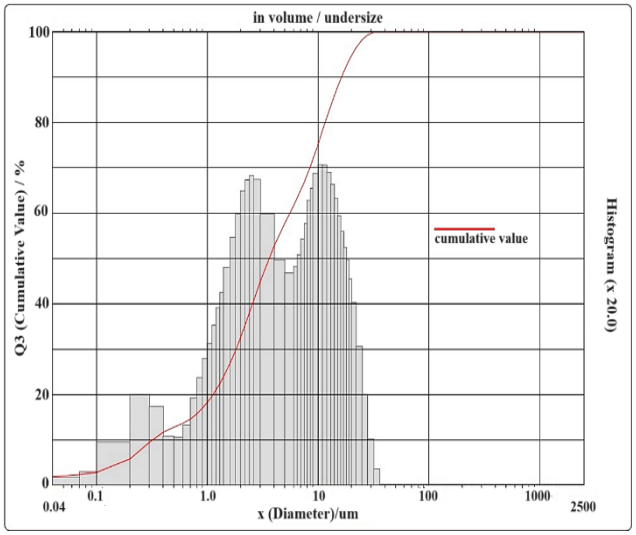

Figure 9. Mean particle size distribution of the resultant ball-milled powder.

The significant increase in the average particle diameter from around 695.6 nm (Table 2) to about 6420 nm (Table 4) suggests that the ball milling process caused particle agglomeration. The mechanical forces generated during milling have led to particles adhering to each other, forming larger clusters. This phenomenon is common in ball mills, where particles are repeatedly subjected to impact, shear, and compression forces [80-82]. The higher PDI value after ball milling (0.831) in Table 4 compared to the initial powder (0.274) in Table 2 indicates a broader distribution of particle sizes, as shown in a histogram in Figure 9. This could be due to the non-uniform nature of the mechanical forces applied during milling, causing uneven agglomeration and dispersion of particles [83,84]. The decrease in the D(10%) value from 500.6 nm (Table 2) to 320 nm (Table 4) suggests the presence of finer particles in the resultant powder after ball milling. These finer particles may be due to the fragmentation of larger agglomerates during milling [82,85-87]. The significant increase in the D(50%) value from 605.6 nm (Table 2) to 3620 nm (Table 4) indicates that the median particle size shifts towards larger sizes. This alignment with the agglomeration phenomenon is observed. The considerable increase in the D(90%) value from 735.5 nm (Table 2) to 16320 nm (Table 4) highlights the formation of a substantial fraction of larger particles. These may be conglomerates of multiple agglomerated particles.

3.4.2 XRD analysis

Figures 10 and Figure 11 depict the diffractograms obtained from the resulting ball-milled powder, which originated from the same powder sample yet underwent distinct XRD tests to ensure accurate compositional analysis. In conjunction with Tables 5 and Table 6, the outcomes of Rietveld analyses verified the presence of lanthanum dihydride (LaH_2) and lanthanum oxide (La_2O_3) within the produced ball-milled powder. Based on the initial XRD assessment (Figure 10 and Table 5), the content of LaH_2 was measured at 71.5%, while La_2O_3 constituted 28.5%. Subsequently, the second XRD measurement (Figure 11 and Table 6) revealed a composition of 68.1% LaH_2 and 31.9% La_2O_3 within the resultant powder.

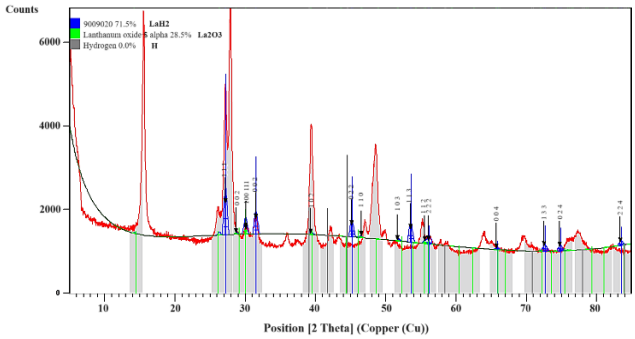

Figure 10. X-ray diffractogram and rietveld analysis from the first XRD measurement of the resultant ball-milled powder. LaH_2 = 71.5% and La_2O_3 = 28.5%.

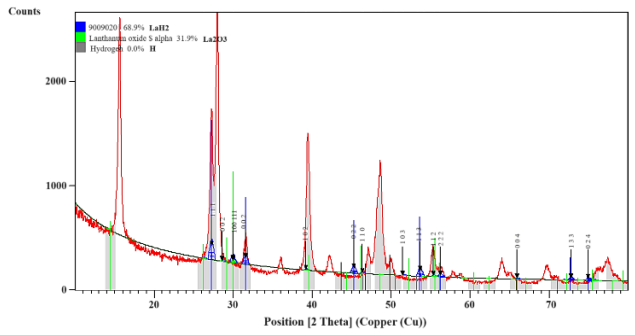

Figure 11. X-ray diffractogram and rietveld analysis from the second XRD measurement of the resultant ball-milled powder. LaH_2 = 68.1% and La_2O_3 = 31.9%.

Table 5. Identified pattern list of the resultant ball-milled powder – the first XRD test.

Visible	Ref. Code	Score	Compound name	Displacement [°2Th.]	Scale factor	Chemical formula
*	96-900-9021	25	9009020	0.000	0.563	$La_{4.00}H_{8.00}$
*	96-101-0279	13	Lanthanum oxide – $-alpha	0.000	0.087	$La_{2.00}O_{3.00}$
*	96-901-1567	5	Hydrogen	0.000	0.284	$H_{2.00}$

Table 6. Identified pattern list of the resultant ball-milled powder – the second XRD test.

Visible	Ref. Code	Score	Compound Name	Displacement [°2Th.]	Scale Factor	Chemical Formula
*	96-900-9021	30	9009020	0.000	0.503	$La_{4.00}H_{8.00}$
*	96-101-0279	5	Lanthanum oxide	0.000	0.329	$La_{2.00}O_{3.00}$
*	96-901-1571	-	Hydrogen	0.000	0.000	$H_{2.00}$
*	96-901-1569	30	Hydrogen	0.000	0.073	$H_{2.00}$

The occurrence of La_2O_3 was associated with the oxidation of LaH_2 powder throughout the stages of pre-milling, milling, and post-milling. The results of the EDX analysis in Figure 6 verified the presence of an oxide layer on the surface of the initial LaH_2 powder. This ball-mill process involved stainless steel balls placed within a sealed milling jar along with the original LaH_2 powder. As the milling jar rotated or vibrated, the balls repeatedly impacted and collided with the powder particles. These collisions created a combination of mechanical stress, friction, and localized heat. The oxide layers present on the surface of the original powder particles might be partially disrupted due to the mechanical forces generated by ball collisions [88,89]. Microscopic cracks, defects, and imperfections in the oxide layer could occur due to the intense impacts. Despite the tightly sealed environment, a small amount of oxygen might still be present within the milling jar. The repeated impacts and particle-to-particle interactions exposed fresh metal surfaces as well as the disrupted oxide layers to this limited oxygen supply. The friction generated by the ball collisions could lead to localized heating of the powder particles. This increase in temperature promoted reactions among the metal surfaces, the disrupted oxide layers, and the available oxygen. The elevated temperature could facilitate the diffusion of oxygen into the cracks and defects within the oxide layers [73]. The exposed metal surfaces and disrupted oxide layers could react with the oxygen present, leading to the further formation of oxide compounds. This oxidation reaction could be particularly enhanced at the sites of mechanical disruptions, cracks, and defects in the original oxide layers [90]. As the ball-mill process continued, the repeated impacts, friction, and localized heating sustained the cycle of oxide layer disruption, exposure to oxygen, and oxidation reactions [91]. This could lead to a gradual increase in the thickness and extent of oxide layers on the powder particles. After the termination of the milling process and the lid was removed, the resultant powder exhibited a minor fire ember (Figure 8) enhancing the formation of oxides.

The possible sequence of chemical reactions that could have taken place:

- Ball-mill process:

$$LaH_2\ (s) + H_2\ (g) \longrightarrow La\ (s) + 2H_2\ (g)$$

In this initial reaction, LaH_2 reacted with hydrogen gas (H_2) from the atmosphere inside the milling jar to produce solid La metal and gaseous hydrogen.

- Spontaneous combustion reaction (after opening the jar lid):

$$4La\ (s) + 3O_2\ (g) \longrightarrow 2La_2O_3\ (s)$$

The La metal produced in the previous step reacted with oxygen (O_2) from the air as the milling jar lid was opened. This exothermic reaction generated heat, and if conditions were right (such as finely divided La metal, oxygen supply, and ignition source), it could lead to spontaneous combustion. The mild fire ember observed could be a result of this reaction.

- Oxidation of LaH_2:

$$LaH_2\ (s) + 2O_2\ (g) \longrightarrow La_2O_3\ (s) + 2H_2O\ (g)$$

The original LaH_2 powder, which already had some oxide layers, further reacted with oxygen from the air, forming La_2O_3 (lanthanum oxide) and water vapor.

The generated water vapor during the reaction could have evaporated due to analysis conditions. XRD is done at controlled room temperature and low humidity, where formed vapor might evaporate before detection. XRD detects crystalline structures; water vapor lacks such structure. Limited water formation due to reaction kinetics, equilibrium, or pathways. Unfavorable reactions or vapor not trapped may evade XRD detection. Sample preparation for XRD might remove initial water content through drying or moisture changes.

In cases like this, it's important to consider that XRD analysis is a powerful tool for determining the crystalline structure of materials, but it might not capture all aspects of a complex reaction system, especially involving gases like water vapor. To gain a more comprehensive understanding of the chemical reactions and their products, complementary techniques like thermal analysis (such as thermo-gravimetric analysis or differential scanning calorimetry) or gas analysis methods could provide additional insights into the formation and behavior of water vapor during the reaction processes.

3.4.3 SEM and EDX analysis

Figures 12(a-d) illustrate the structure of the powder obtained through ball milling, under 100×, 1500×, 2500×, and 5000× magnifications. This powder predominantly exhibits spherical and rounded forms, regardless of their dimensions. Considering the average size of the powder after ball milling, which is 6420 nm (Table 4), this observation potentially suggests that the powder displayed in Figure 12 could fall within the D(10%) and D(50%) percentiles, with an average size of 320 nm and 3620 nm respectively, as indicated in Table 4. A large particle was observed in Figure 12(a) (blue arrow) showing an example of particle size beyond the D(90%) percentile.

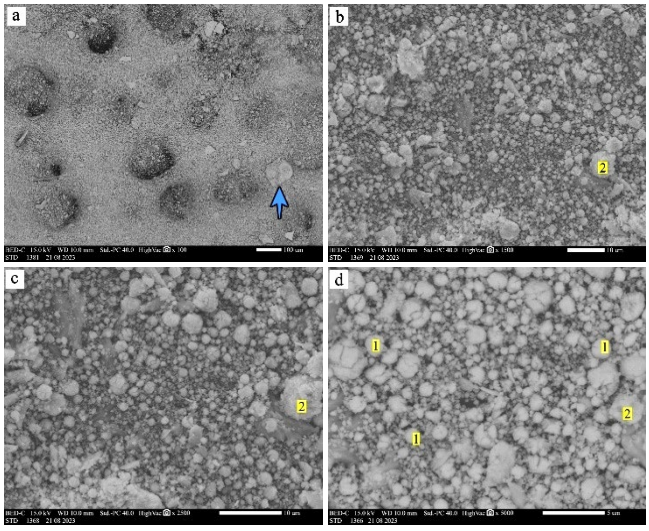

Figure 12. The morphology of the resultant ball-milled powder under SEM observation: (a) 100×, (b) 1500×, (c) 2500×, and (d) 5000×. The shapes of the powder were predominantly spherical (1) and rounded (2), regardless of size.

Table 7. EDX spectrum of the resultant ball-milled powder.

Element	Line	Weight%	Atom%
O	K	32.03 ± 0.08	80.36 ± 0.20
La	L	67.97 ± 0.19	19.64 ± 0.05
Total		100.00	100.00
		Map_001_wholespectrum	Fitting ratio 0.1817

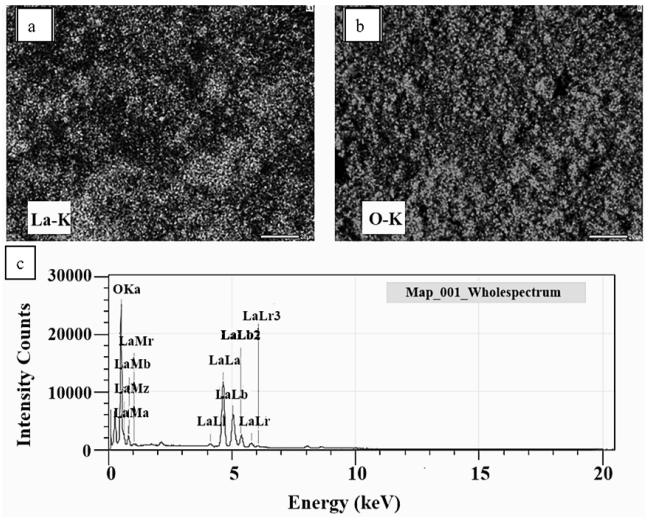

Figure 13. The results of EDX analysis on the resultant ball-milled powder (magnification: 800×): (a) Lanthanum (green areas), (b) Oxygen (red areas), and (c) EDX total spectrum.

The observed rounded or circular shape in Figure 12 could be influenced by several factors. Given the initial shapes of the powder before the ball mill (rounded, angular, acicular, and flaky), the transformation to rounded or circular shapes could be attributed to the ball mill process itself, while the oxidation might modify the surface properties without drastically altering the overall morphology. The initial powder with various shapes might have undergone plastic deformation during the ball mill, causing the particles to round out or become more spherical [92-94]. This could occur as a result of shearing forces and particle-to-particle collisions [95,96]. Oxidation primarily affects the outermost layers of particles. The oxidized layer can form due to reactions with oxygen in the environment. While oxidation might lead to changes in the chemical composition of the surface, it may not significantly alter the overall shape of the particles, especially if the deformation induced during the ball mill has already shaped them into more rounded or circular forms. However, the formation of oxides on the surface might have smoothing effects, further enhancing the appearance of rounded shapes [97,98]. Oxidation might also alter the surface energy and interactions between particles, influencing how they aggregate and adhere [99,100]. It's possible that the combined effects of the ball mill and subsequent oxidation were responsible for the observed rounded or circular shapes in the resultant ball-milled powder. The mechanical forces from the ball mill could initiate the reshaping process, and oxidation might refine and enhance the formed shapes.

Figures 13(a-c) along with Table 7 present the outcomes derived from EDX mapping analysis performed on the resultant ball-milled powder. The quantification of oxygen content at 32.03 ± 0.08 wt% or 80.36 ± 0.20 at% provides corroborative evidence of the oxidation phenomenon within the obtained powder. As previously expounded, the oxidation process of LaH_2 powder demonstrated intricacies arising from the interplay of mechanical forces and localized heat engendered during the ball-milling procedure. The intricate dynamics involved the establishment and disruption of oxide layers on the powder's surface, coupled with the constricted availability of oxygen. The recurring occurrences of particle collisions and interactions facilitated the exposure of disrupted oxide layers to oxygen, thereby fostering oxidation reactions. The confluence of mechanical perturbation, oxygen contact, and localized heating culminated in a gradual augmentation of oxide layer thickness and coverage on the particles. Furthermore, the emergence of a minor fire ember after milling termination served to augment the progression of oxide formation.

In Figure 13 and Table 7, the presence of LaH_2 is identified through its detection as La. However, the analysis of samples containing hydrogen, such as LaH_2 powder, faces intrinsic limitations that hinder effective hydrogen detection. The low atomic number of hydrogen leads to feeble X-ray emissions and shallow penetration, which makes distinguishing hydrogen signals from background noise challenging and impedes accurate measurement. EDX detectors, designed for higher-energy X-rays, demonstrate reduced sensitivity to hydrogen detection. The adherence of hydrogen onto surfaces, originating from both the sample's surroundings and handling procedures, introduces potential interference. Complexities arising from background correction and detector response at low energies further complicate the precise quantification of hydrogen, consequently introducing uncertainties in the quantified hydrogen content.

4. Conclusion

A comprehensive investigation was conducted into the behavior of LaH_2 during ball milling, revealing significant mechanical, chemical, and morphological changes. Through meticulous experimentation, the intricate relationship between milling time and hydrogen pressure reduction was elucidated, highlighting the dynamic nature of the process. The observation of a minor fire ember upon unsealing the milling jar post-milling underscored the complex interplay between mechanical forces and chemical reactivity within the LaH_2 powder. Utilizing advanced analytical techniques including X-ray diffraction (XRD), scanning electron microscopy coupled with energy-dispersive X-ray spectroscopy (SEM/EDX), and particle size distribution analysis, profound alterations in the structure, composition, and morphology of the milled powder were unveiled. A dual-phase composition comprising lanthanum dihydride (LaH_2) and lanthanum oxide (La_2O_3), indicative of a dynamic chemical equilibrium during milling, was demonstrated. Moreover, the characterization of particle size distribution highlighted a significant increase in average diameter and polydispersity index (PDI), reflecting extensive particle agglomeration and plastic deformation. Insights into the morphological evolution of the powder were provided

through SEM imaging, revealing predominantly spherical and rounded forms, characteristic of particle agglomeration. Additionally, the formation of oxide layers on the powder surface was elucidated through EDX mapping, contributing further to the understanding of morphological evolution during milling. In summary, the findings advanced the understanding of LaH_2 behavior under extreme mechanical and chemical conditions, with implications for materials processing, hydrogen storage technologies, and broader applications in materials science and engineering. By unraveling the intricate dynamics of LaH_2 during ball milling, this study laid the groundwork for optimizing materials synthesis and processing techniques in future research endeavors.

Acknowledgments

The authors would like to thank E-Layanan Sains (ELSA), National Research and Innovation Agency (BRIN) Indonesia, for providing the facilities, and scientific, as well as technical support for this research.

References

[1] S. Raha, and Md. Ahmaruzzaman, "ZnO nanostructured materials and their potential applications: Progress, challenges, and perspectives," *Nanoscale Advances*, vol. 4, no. 8, pp. 1868-1925, 2022

[2] S. Yadav, R. Dixit, S. Sharma, S. Dutta, K. Solanki, and R. K. Sharma, "Magnetic metal–organic framework composites: Structurally advanced catalytic materials for organic transformations," *Materials Advances*, vol. 2, no. 7, pp. 2153-2187, 2021

[3] R. K. Sharma, S. Yadav, S. Dutta, H. B. Kale, I. R. Warkad, R. Zboril, R. S. Varma, and M. B. Gawande, "Silver nanomaterials: Synthesis and (electro/photo) catalytic applications," *Chemical Society Reviews*, vol. 50, no. 20, pp. 11293-11380, 2021.

[4] S. L. James, and T. Friščić, "Mechanochemistry," *Chemical Society Review*, vol. 42, no. 18, p. 7494, 2013.

[5] T. Friščić, C. Mottillo, and H. M. Titi, "Mechanochemistry for synthesis," *Angewandte Chemie*, vol. 132, no. 3, pp. 1030-1041, .2020.

[6] X. Liu, Y. Li, L. Zeng, X. Li, N. Chen, S. Bai, H. He, Q. Wang, and C. Zhang, "A review on mechanochemistry: Approaching advanced energy materials with greener force," *Advanced Materials*, vol. 34, no. 46, p. 2108327, 2022.

[7] D. Tan, and F. García, "Main group mechanochemistry: From curiosity to established protocols," *Chemical Society Reviews*, vol. 48, no. 8, pp. 2274-2292, 2019.

[8] L. Pasquini, K. Sakaki, E. Akiba, M. D. Allendorf, E. Alvares, J. R. Ares, D. Babai, M. Baricco, J. Beelosta von Colbe, M. Bereznitsky, C. E. Buckley, Y. W. Cho, F. Cuevas, P. de Rango, E. M. Dematteis, R. V. Denys, M. Dornheim, J. F. Fernandez, A. Harivadi, B. C. Hauback, T. W. Heo, M. Hirscher, T. D. Humphries, J. Huot, I. Jacob, T. R. Jensen, P. Jerabek, S. Y. Kang, N. Keilbart, H. Kim, M. Latroche, F. Leardini, H. Li, S. Ling, M. V. Lototskyv, R. Mullen, S-i. Orimo, M. Paskevicius, C. Pistidda, M. Polanski, J. Puszkiel, E. Rabkin, M. Sahlberg, S. Sartori, A. Santhosh, R. Z. Shneck, M. H. Sorby, Y. Shang, V. Stavila. J-Y. Suh, S. Suwamo, L. Thi Thu, L. F. Wan, C. J. Webb, M. Witman, C. Wan, B. C. Wood, and V. A. Yarys, "Magnesium- and intermetallic alloys-based hydrides for energy storage: Modelling, synthesis and properties," *Progress in Energy*, vol. 4, no. 3, p. 032007, 2022.

[9] S. Mateti, M. Mathesh, Z. Liu, T. Tao, T. Ramireddy, A. M. Glushenkov, W. Yang, and Y. lan Chen, "Mechanochemistry: A force in disguise and conditional effects towards chemical reactions," *Chemical Communications*, vol. 57, no. 9, pp. 1080-1092, 2021

[10] P. Cai, C. Wang, H. Gao, and X. Chen, "Mechanomaterials: A rational deployment of forces and geometries in programming functional materials," *Advanced Materials*, vol. 33, no. 46, p. 2007977, 2021.

[11] P. Dulian, "Solid-state mechanochemical syntheses of perovskites," in *Perovskite Materials: Synthesis, Characterisation, Properties, and Applications*, vol. 1, L. Pan and G. Zhu, Eds., Rijeka, Croatia: IntechOpen, 2016, pp. 3-26.

[12] V. Martinez, T. Stolar, B. Karadeniz, I. Brekalo, and K. Užarević, "Advancing mechanochemical synthesis by combining milling with different energy sources," *Nature Reviews Chemistry*, vol. 7, no. 1, pp. 51-65, 2022.

[13] G.-F. Han, F. Li, Z. W. Chen, C. Coppex, S-J. Kim, H-J. Noh, Z. fu. Y. Lu, C. V. Singh, S. Siahrostami, Q. Jiang, and J-B. Baek, "Mechanochemistry for ammonia synthesis under mild conditions," *Nature Nanotechnology*, vol. 16, no. 3, pp. 325-330, Mar. 2021.

[14] Y. Li, A. R. Zimmerman, F. He, J. Chen, L. Han, H. Chen X. Hu, and B. Gao, "Solvent-free synthesis of magnetic biochar and activated carbon through ball-mill extrusion with Fe3O4 nanoparticles for enhancing adsorption of methylene blue," *Science of The Total Environment*, vol. 722, p. 137972, . 2020.

[15] J.-L. Do, and T. Friščić, "Chemistry 2.0: Developing a new, solvent-free system of chemical synthesis based on mechanochemistry," *Synlett*, vol. 28, no. 16, pp. 2066-2092, . 2017.

[16] J. Cantway, "Solvent-free synthesis of metal coordination compounds using ball mills," Master Thesis, Western Kentucky University, Bowling Green, Kentucky, 2020.

[17] K. Ariga, T. Mori, and J. P. Hill, "Mechanical control of nanomaterials and nanosystems," *Advanced Materials*, vol. 24, no. 2, pp. 158-176, 2012.

[18] E. Gaffet, and G. Le Caer, "Mechanical processing for nanomaterials," in *Encyclopedia of Nanoscience and Nanotechnology*, vol. 10, H. S. Nalwa, Ed., American Scientific Publishers, 2004, pp. 1-39.

[19] T. Tsuzuki, "Mechanochemical synthesis of metal oxide nanoparticles," *Communications Chemistry*, vol. 4, no. 1, p. 143, 2021.

[20] M. Wang, W. Bi, X. Huang, and D. D. Y. Chen, "Ball mill assisted rapid mechanochemical extraction method for natural products from plants," *Journal of Chromatography A*, vol. 1449, pp. 8-16, Jun. 2016.

[21] S. Głowniak, B. Szczęśniak, J. Choma, and M. Jaroniec, "Mechanochemistry: Toward green synthesis of metal-organic frameworks," *Materials Today*, vol. 46, pp. 109-124, 2021.

[22] F. Chemat, M. Vian, A-S. Fabiano-Tixier, M. Nutrizio, A. R. Jambrak, P. E. Munekata, J. M. Lorenzo, F. J. Barba, A. Binello, and G. Cravotto, "A review of sustainable and intensified techniques for extraction of food and natural products," *Green Chemistry*, vol. 22, no. 8, pp. 2325-2353, 2020.

[23] M. Q. Farooq, N. M. Abbasi, and J. L. Anderson, "Deep eutectic solvents in separations: Methods of preparation, polarity, and applications in extractions and capillary electrochromatography," *Journal of Chromatography A*, vol. 1633, p. 461613, . 2020.

[24] E. S. M. El-Sayed, and D. Yuan, "Reticular design and synthesis strategies of metal-organic frameworks," in *Reticular Chemistry and Applications: Metal-Organic Frameworks*, vol. 11, Y. Belmabkhout and K. E. Cordova, Eds., Walter de Gruyter GmbH & Co KG, 2023, pp. 11-17.

[25] S. A. Younis, N. Bhardwaj, S. K. Bhardwaj, K.-H. Kim, and A. Deep, "Rare earth metal–organic frameworks (RE-MOFs): Synthesis, properties, and biomedical applications," *Coordination Chemistry Reviews*, vol. 429, p. 213620, 2021.

[26] F. Palazon, Y. El Ajjouri, and H. J. Bolink, "Making by grinding: Mechanochemistry boosts the development of halide perovskites and other multinary metal halides," *Advanced Energy Materials*, vol. 10, no. 13, p. 1902499, 2020.

[27] J. Martí-Rujas, "Structural elucidation of microcrystalline MOFs from powder X-ray diffraction," *Dalton Transactions*, vol. 49, no. 40, pp. 13897-13916, 2020.

[28] X. Zhang, J. Zheng, Y. Wang, Z. Wang, L. Zheng, A. Nozariasbarz, K. Tao, B. Ma, B. Poudel, K. Wang, and T. Ye, "Solvent-free synthetic protocols for halide perovskites," *Inorganic Chemistry Frontiers*, vol. 10, no. 12, pp. 3468-3488, 2023.

[29] P. Ying, J. Yu, and W. Su, "Liquid-assisted grinding mechano-chemistry in the synthesis of pharmaceuticals," *Advanced Synthesis Catalysis*, vol. 363, no. 5, pp. 1246-1271, 2021.

[30] P. Baláž, M. Baláž, M. Achimovičová, Z. Bujňáková, and E. Dutková, "Chalcogenide mechanochemistry in materials science: insight into synthesis and applications (a review)," *Journal of Materials Science*, vol. 52, no. 20, pp. 11851-11890, 2017.

[31] S. Zhang, Q. Yang, C. Wang, X. Luo, J. Kim, Z. Wang, Y. Yamauchi,"Porous organic frameworks: Advanced materials in analytical chemistry," *Advanced Science*, vol. 5, no. 12, p. 1801116, 2018.

[32] K. J. Ardila-Fierro, and J. G. Hernández, "Sustainability assessment of mechanochemistry by using the twelve principles of green chemistry," *ChemSusChem*, vol. 14, no. 10, pp. 2145-2162, 2021.

[33] R. B. N. Baig, and R. S. Varma, "Alternative energy input: mechanochemical, microwave and ultrasound-assisted organic synthesis," *Chemical Society Reviews*, vol. 41, no. 4, pp. 1559-1584, 2012.

[34] R. S. Varma, "Journey on greener pathways: from the use of alternate energy inputs and benign reaction media to sustainable applications of nano-catalysts in synthesis and environmental remediation," *Green Chemistry*, vol. 16, no. 4, p. 2027, 2014.

[35] M. Hirscher, V. A. Yartys, M. Baricco, J. M. Bellosta von Colbe, D. Blanchard, R. Bowman, D. P. Broom, C. E. Buckley, F. Chang, P. Chen, Y. W. Cho, J-C. Crivello, F. Cuevas, W. I. F. David, P. E. de Jongh, R. Denys, M. Dornheim, M. Felderhoff, Y. Filinchuk, G. E. Froudakis, D. M. Grant, E. M. Gray, B. C. Hauback, T. He, T. D. Humphries, T. R. Jensen, S. Kim, Y. Kojima, M. Latroche, L. Hai-Wen, M. V. Lototskyy, J. W. Makepeace, K. T. Moller, L Naheed, P. Ngene, D. Noreus, M. M. Nygard, O. Shin-ichi, M. Paskevicius, L. Pasquini, D. B. Ravnsbaek, M. V. Sofianos, T. J. Udovic, T. Vegge, G. S. Walker, C. J. Webb, C. Weidenthaler, and C. Zlotea, "Materials for hydrogen-based energy storage – past, recent progress and future outlook," *Journal of Alloys and Compounds*, vol. 827, p. 153548, 2020.

[36] S. K. Gupta, and P. K. Jha, "Dynamical stability of the lanthanum dihydride under high pressure: A density functional lattice dynamics approach," *International Journal of Hydrogen Energy*, vol. 38, no. 11, pp. 4654-4663, 2013.

[37] A. Machida, T. Watanuki, D. Kawana, and K. Aoki, "Phase separation of lanthanum hydride under high pressure," *Physical Review B*, vol. 83, no. 5, p. 054103, 2011.

[38] D. Tang, G-L. Tan, G-W. Li, J-G. Liang, S. M. Ahmad, A. Bahadur, M. Humayun, H. Ullah, A. Khan, and M. Bououdina, "State-of-the-art hydrogen generation techniques and storage methods: A critical review," *Journal of Energy Storage*, vol. 64, p. 107196, 2023.

[39] Q. Hassan, I. D. J. Azzawi, A. Z. Sameen, and H. M. Salman, "Hydrogen fuel cell vehicles: Opportunities and challenges," *Sustainability*, vol. 15, no. 15, p. 11501, 2023.

[40] P. Ragupathy, S. D. Bhat, and N. Kalaiselvi, "Electrochemical energy storage and conversion: An overview," *WIREs Energy and Environment*, vol. 12, no. 2, 2023.

[41] F. Schüth, "Challenges in hydrogen storage," *The European Physical Journal Special Topics*, vol. 176, no. 1, pp. 155-166, Sep. 2009.

[42] S. Dunn, "Hydrogen futures: toward a sustainable energy system," *International Journal of Hydrogen Energy*, vol. 27, no. 3, pp. 235-264, 2002.

[43] V. Sethi, X. Sun, D. Nalianda, A. Rolt, P. Holborn, C. Wijesinghe, C. Xisto, I. J. H. Jonsson, T. Gronstedt J. M. Ingram, A. Lundbladh, A. T. Isikveren, I. Williamson, T. Harrison, and A. Yenokyan, "Enabling cryogenic hydrogen-based CO_2-free air transport: Meeting the demands of zero carbon aviation," *IEEE Electrification Magazine*, vol. 10, no. 2, pp. 69-81, 2022..

[44] T. Huebert, L. Boon-Brett, and W. J. Buttner, *Sensors for safety and process control in hydrogen technologies*. Boca Raton, Florida: CRC Press, 2016.

[45] A. Iskandarov, T. Tada, S. Iimura, and H. Hosono, "Characteristic mechanism for fast H− conduction in LaH2.5O0.25," *Acta Materialia*, vol. 230, p. 117825, 2022.

[46] Y. Sakurai, A. Machida, and K. Aoki, "Vibrational spectroscopy studies of a pressure-induced disproportionation reaction of LaH_2," *Solid State Communications*, vol. 151, no. 11, pp. 815-817, 2011.

[47] I. G. Ratishvili, and P. Vajda, "Hydrogen ordering in super-stoichiometric rare-earth hydrides for a system with an energy-constants ratio p = V2/V1<1: LaH2+x," *Physical Review B*, vol. 53, no. 2, pp. 581-587, 1996.

[48] J. Kleperis, G. Wójcik, A. Czerwinski, J. Skowronski, M. Kopczyk, and M. Beltowska-Brzezinska, "Electrochemical behavior of metal hydrides," *Journal of Solid State Electrochemistry*, vol. 5, no. 4, pp. 229-249, 2001.

[49] Ch. Christodoulou, G. Karagiorgis, A. Poullikkas, N. Lymberopoulos, and E. Varkaraki, "A review on hydrogen storage technologies," *The Cyprus Journal of Science and Technology*, vol. 4, no. 3, pp. 72-144, 2005.

[50] J. Fan, Z. Yang, and S. Dai, "Construction of conjugated scaffolds driven by mechanochemistry towards energy storage applications," *Green Chemical Engineering*, 2023.

[51] Samriti, R. Tyagi, O. Ruzimuradov, and J. Prakash, "Fabrication methods and mechanisms for designing highly-efficient photo-catalysts for energy and environmental applications," *Materials Chemistry and Physics*, vol. 307, p. 128108, 2023.

[52] R. Dubadi, S. D. Huang, and M. Jaroniec, "Mechanochemical synthesis of nanoparticles for potential antimicrobial applications," *Materials*, vol. 16, no. 4, p. 1460, 2023.

[53] F. Cuccu, L. De Luca, F. Delogu, E. Colacino, N. Solin, R. Mocci, and A. Porcheddu, "Mechanochemistry: New tools to navigate the uncharted territory of 'impossible' reactions," *ChemSusChem*, vol. 15, no. 17, 2022.

[54] Z. Yin, Q. Zhang, S. Li, G. Cagnetta, J. Huang, S. Deng, and G. Yu, "Mechanochemical synthesis of catalysts and reagents for water decontamination: Recent advances and perspective," *Science of The Total Environment*, vol. 825, p. 153992, 2022.

[55] F. Delogu, G. Gorrasi, and A. Sorrentino, "Fabrication of polymer nanocomposites via ball milling: Present status and future perspectives," *Progress Materials Science*, vol. 86, pp. 75-126, 2017.

[56] Q. Li, Y. Lu, Q. Luo, X. Yang, Y. Yang, J. Tan, Z. Dong, J. Dang, J. Li, Y. Chen, B. Jiang, S. Sun, and F. Pan, "Thermodynamics and kinetics of hydriding and dehydriding reactions in Mg-based hydrogen storage materials," *Journal of Magnesium and Alloys*, vol. 9, no. 6, pp. 1922-1941, 2021.

[57] N. Abid, A. M. Khan, S. Shujait, K. Chaudhary, M. Ikram, M. Imron, J. Haider, M. Khan, Q. Khan, and M. Maqbool, "Synthesis of nanomaterials using various top-down and bottom-up approaches, influencing factors, advantages, and disadvantages: A review," *Advances in Colloid and Interface Science*, vol. 300, p. 102597, 2022.

[58] C. Suryanarayana, A. A. Al-Joubori, and Z. Wang, "Nano-structured materials and nanocomposites by mechanical alloying: An overview," *Metals and Materials International*, vol. 28, no. 1, pp. 41-53, 2022.

[59] C. Shuai, C. He, S. Peng, F. Qi, G. Wang, A. Min, W. Yang, and W. Wang, "Mechanical alloying of immiscible metallic systems: Process, microstructure, and mechanism," *Advanced Engineering Materials*, vol. 23, no. 4, p. 2001098, 2021.

[60] M. A. Meyers, A. Mishra, and D. J. Benson, "Mechanical properties of nanocrystalline materials," *Progress in Materials Science*, vol. 51, no. 4, pp. 427-556, 2006.

[61] R. Daassi, K. Durand, D. Rodrigue, and T. Stevanovic, "Optimization of the electrospray process to produce lignin nanoparticles for PLA-based food packaging," *Polymers (Basel)*, vol. 15, no. 13, p. 2973, 2023.

[62] M. J. Masarudin, S. M. Cutts, B. J. Evison, D. R. Phillips, and P. J. Pigram, "Factors determining the stability, size distribution, and cellular accumulation of small, monodisperse chitosan nanoparticles as candidate vectors for anticancer drug delivery: application to the passive encapsulation of [14C]-doxorubicin," *Nanotechnology Science and Applications*, vol. 8, pp. 67-80, 2015.

[63] G. Ren, H. Su, and S. Wang, "The combined method to synthesis silica nanoparticle by Stöber process," *Journal of Sol-Gel Science and Technology*, vol. 96, no. 1, pp. 108-120, 2020.

[64] J. G. Whiting, E. J. Garboczi, V. N. Tondare, J. H. J. Scott, M. A. Donmez, and S. P. Moylan, "A comparison of particle size distribution and morphology data acquired using lab-based and commercially available techniques: Application to stainless steel powder," *Powder Technology*, vol. 396, pp. 648-662, 2022.

[65] H. Runyan, R. A. Reynolds, and D. Stramski, "Evaluation of particle size distribution metrics to estimate the relative contributions of different size fractions based on measurements in Arctic waters," *Journal of Geophysical Research: Oceans*, vol. 125, no. 6, 2020.

[66] H. G. Merkus, "Particle size, size distributions, and shape," in *Particle Size Measurements: Fundamentals, Practice, Quality*, Springer Dordrecht, 2009, pp. 13-42.

[67] A. Machida, T. Watanuki, D. Kawana, and K. Aoki, "Disproportionation reaction of LaH_2 at high pressure and low temperature," *Journal of Physics: Conference Series*, vol. 500, no. 2, p. 022001, 2014.

[68] E. Boroch, K. Conder, C. Ru-Xiu, and E. Kaldis, "An X-ray investigation of the phase relationships in the system LaH_2 LaH3," *Journal of the Less Common Metals*, vol. 156, no. 1-2, pp. 259–271, 1989.

[69] H. M. Beakawi Al-Hashemi and O. S. Baghabra Al-Amoudi, "A review on the angle of repose of granular materials," *Powder Technology*, vol. 330, pp. 397-417, 2018.

[70] N. J. John, I. Khan, S. Kandalai, and A. Patel, "Particle breakage in construction materials: A geotechnical perspective," *Construction and Building Materials*, vol. 381, p. 131308, Jun. 2023.

[71] N. C. Balaji, M. Mani, and B. V. V. Reddy, "Discerning heat transfer in building materials," *Energy Procedia*, vol. 54, pp. 654-668, 2014.

[72] A. Nouri, and A. Sola, "Metal particle shape: A practical perspective," *Metal Powder Report*, vol. 73, no. 5, pp. 276-282, 2018.

[73] S. R. J. Saunders, M. Monteiro, and F. Rizzo, "The oxidation behavior of metals and alloys at high temperatures in atmospheres containing water vapor: A review," *Progress in Materials Science*, vol. 53, no. 5, pp. 775-837, 2008.

[74] A. S. Khanna, "High-temperature oxidation," in *Handbook of Environmental Degradation of Materials*, Elsevier, 2005, pp. 105–152.

[75] G. Liang, S. Boily, J. Huot, A. V. Neste, and R. Schulz, "Hydrogen absorption properties of a mechanically milled Mg–50 wt% LaNi5 composite," *Jourenal of Alloys and Compounds*, vol. 268, no. 1–2, pp. 302-307, 1998.

[76] J. N. Huiberts, R. Griessen, J. H. Rector, R. J. Wijngaarden, J. P. Dekker, D. G. de Groot, and N. J. Koeman, "Yttrium and lanthanum hydride films with switchable optical properties," *Nature*, vol. 380, no. 6571, pp. 231-234, 1996.

[77] E. J. Goon, "The non-stoichiometry of lanthanum hydride," *Journal of Physical Chemistry*, vol. 63, no. 12, pp. 2018-2021, 1959.

[78] M. Pozzo, and D. Alfè, "Hydrogen dissociation and diffusion on transition metal (=Ti, Zr, V, Fe, Ru, Co, Rh, Ni, Pd, Cu, Ag)-doped Mg(0001) surfaces," *International Journal of Hydrogen Energy*, vol. 34, no. 4, pp. 1922-1930, 2009.

[79] M. Pozzo, D. Alfè, A. Amieiro, S. French, and A. Pratt, "Hydrogen dissociation and diffusion on Ni- and Ti-doped Mg(0001) surfaces," *Journal of Chemical Physics*, vol. 128, no. 9, 2008.

[80] R. Xu, Z. Tan, D-B. Xiong, G. Fan, Q. Guo, J. Zhang, Y. Su, Z. Li, and D. Zhang, "Balanced strength and ductility in CNT/Al composites achieved by flake powder metallurgy via shift-speed ball milling," *Composites Part A Applied Science and Manufacturing*, vol. 96, pp. 57-66, 2017.

[81] L. Lu, and M. O. Lai, *Mechanical alloying*. Boston, Dordrecht, London: Kluwer Academic Publishers, 1998.

[82] S. A. Hewitt, and K. A. Kibble, "Effects of ball milling time on the synthesis and consolidation of nanostructured WC–Co composites," *International Journal of Refractory Metals Hard Materials*, vol. 27, no. 6, pp. 937-948, 2009.

[83] T. Singh, S. K. Tiwari, and D. K. Shukla, "Novel method of nanoparticle addition for friction stir welding of aluminum alloy," *Advances in Materials and Processing Technologies*, vol. 8, no. 1, pp. 1160-1172, 2022.

[84] N. N. Obradović, W. G. Fahenholtz, S. Filipovic, D. Kosanovic, A. Dapcevic, A. Dordevic, I. Balac, and V. B. Pavlovic,"The effect of mechanical activation on synthesis and properties of $MgAl_2O_4$ ceramics," *Ceramics International*, vol. 45, no. 9, pp. 12015-12021, 2019.

[85] N. Le Bolay, "On agglomeration phenomena in ball mills: application to the synthesis of composite materials," *Powder Technology*, vol. 130, no. 1-3, pp. 450-455, 2003.

[86] M.-G. Li, C.-J. Sun, S.-H. Gau, and C.-J. Chuang, "Effects of wet ball milling on lead stabilization and particle size variation in municipal solid waste incinerator fly ash," *Journal of Hazardous Materials*, vol. 174, no. 1-3, pp. 586-591, 2010.

[87] Q. Fang, and Z. Kang, "An investigation on morphology and structure of Cu–Cr alloy powders prepared by mechanical milling and alloying," *Powder Technology*, vol. 270, pp. 104-111, 2015.

[88] C. Suryanarayana, "Mechanical alloying and milling," *Mechanical Alloying and Milling*, vol. 46, pp. 1-472, 2004.

[89] T. Prasad Yadav, R. Manohar Yadav, and D. Pratap Singh, "Mechanical milling: A top-down approach for the synthesis of nanomaterials and nanocomposites," *Nanoscience and Nanotechnology*, vol. 2, no. 3, pp. 22-48, 2012.

[90] N. Ao, D. Liu, X. Zhang, and C. Liu, "Enhanced fatigue performance of modified plasma electrolytic oxidation coated Ti-6Al-4V alloy: Effect of residual stress and gradient nano-structure," *Applied Surface Science*, vol. 489, pp. 595-607, Sep. 2019.

[91] L. Takacs, "Self-sustaining reactions induced by ball milling," *Progress in Materials Science*, vol. 47, no. 4, pp. 355-414, 2002.

[92] B. Fullenwider, P. Kiani, J. M. Schoenung, and K. Ma, "Two-stage ball milling of recycled machining chips to create an alternative feedstock powder for metal additive manufacturing," *Powder Technology*, vol. 342, pp. 562-571, 2019.

[93] M. Ramezani, and T. Neitzert, "Mechanical milling of aluminum powder using planetary ball milling process," *Journal of Achievements in Materials and Manufacturing Engineering*, vol. 55, no. 2, pp. 790-798, 2012.

[94] M. Toozandehjani, K. Matori, F. Ostovan, S. Abdul Aziz, and M. Mamat, "Effect of milling time on the microstructure, physical, and mechanical properties of Al-Al_2O_3 nanocomposite synthesized by ball milling and powder metallurgy," *Materials*, vol. 10, no. 11, p. 1232, 2017.

[95] S. Kim, and W. S. Choi, "Analysis of ball movement for research of grinding mechanism of a stirred ball mill with 3D discrete element method," *Korean Journal of Chemical Engineering*, vol. 25, no. 3, pp. 585-592, 2008.

[96] P. Muhayimana, J. K. Kimotho, and H. M. Ndiritu, "A review of ball mill grinding process modeling using discrete element method," in *Proceedings of the Sustainable Research and Innovation (SRI) Conference*, 2022, pp. 221-229.

[97] X. Zhu, J. Chen, L. Scheideler, R. Reichl, and J. Geis-Gerstorfer, "Effects of topography and composition of titanium surface oxides on osteoblast responses," *Biomaterials*, vol. 25, no. 18, pp. 4087-4103, 2004.

[98] N. A. Che Lah, A. Kamaruzaman, and S. Trigueros, "pH-dependent formation of oriented zinc oxide nanostructures in the presence of tannic acid," *Nanomaterials*, vol. 11, no. 1, p. 34, 2020.

[99] M. Kušter, J. Kovac, Z. Samardzija, M. Komelj, S. S. Parapari, M. Podlogar, J-M. Dubois, and S. Sturm,"Impact of tuned oxidation on the surface energy of sintered samples produced from atomized B-doped Al-Cu-Fe quasicrystalline powders," *Crystals (Basel)*, vol. 13, no. 6, p. 859, 2023.

[100] S. Mangal, F. Meiser, G. Tan, T. Gengenbach, D. A. V. Morton, and I. Larson, "Applying surface energy derived cohesive–adhesive balance model in predicting the mixing, flow and compaction behavior of interactive mixtures," *European Journal of Pharmaceutics and Bioplarm,* vol. 104, pp. 110-116, 2016.